*Chinese Journal of*
**POLYMER SCIENCE**

RESEARCH ARTICLE

https://doi.org/10.1007/s10118-025-3547-8
*Chinese J. Polym. Sci.* **2026**, *44*, 768–780

# Strong and Tough Composite Hydrogels with Crack-deflecting Ability Enabled by a Viscoelastoplastic Mixing Strategy

Xiang Li†, Bei Jiang†, Bin Wang, Ya-Rong Yang, Gui-Ming Zhao, and Li-Li Wang*

*State Key Laboratory of Bio-Fibers and Eco-Textiles, College of Materials Science and Engineering, Qingdao University, Qingdao 266071, China*

Electronic Supplementary Information

**Abstract** The weak interfacial bonding and significant modulus mismatch between the reinforcement phase and the hydrogel matrix greatly limit the reinforcing efficiency in conventional composite hydrogels. To address these issues, we propose a novel design strategy based on dynamic mechanical control, summarized as "blending reinforcement in the viscoelastoplastic state and fixing the structure in the viscoelastic state." This approach utilizes a unique poly(vinyl alcohol) (PVA) hydrogel matrix featuring an amorphous/strong hydrogen-bonding hierarchical architecture, which undergoes a thermal-induced transition from a viscoelastoplastic to a viscoelastic state, enabling effective filler dispersion and subsequent structural stabilization. The method effectively suppresses filler aggregation through mechanical mixing in the viscoelastoplastic matrix, while the high polymer chain density and abundant physical interactions reduce modulus mismatch between dual phases. This synergy, together with enhanced interfacial strength achieved through strong physical bonding and structural reorganization during the cooling-induced mechanical transition, creates a robust interface that promotes crack deflection and tortuous crack propagation. As a result, we successfully fabricate PVA/silica composite hydrogels with outstanding mechanical properties and long-term stability. Moreover, by leveraging the salt-responsive nature of the system, the mechanical properties of the composite hydrogels can be reversibly and broadly modulated *via* a salt solution exchange strategy. This work establishes a fundamental principle and a practical pathway for the design and fabrication of advanced hydrogel composites.

**Keywords** Poly(vinyl alcohol) hydrogel; Interfacial bonding; Mechanical properties

**Citation:** Li, X.; Jiang, B.; Wang, B.; Yang, Y. R.; Zhao, G. M.; Wang, L. L. Strong and tough composite hydrogels with crack-deflecting ability enabled by a viscoelastoplastic mixing strategy. *Chinese J. Polym. Sci.* **2026**, *44*, 768–780.

## INTRODUCTION

In recent years, the application of flexible materials in areas such as tissue engineering scaffolds and wearable electronic devices[1,2] has spurred significant growth in the development of advanced composite materials that integrate mechanical strength with dynamic responsive properties.[3–6] Among these, hydrogels have become a leading matrix for novel soft materials because they form stable, tunable cross-linked networks and offer superb mechanical flexibility, high biocompatibility, and straightforward processability.[7–10] However, the single-crosslinked networks of traditional hydrogels inherently exhibit a narrow range of mechanical properties,[11] this makes it difficult to achieve the synergistic combination of high strength and toughness required for dynamic, high-load applications.

To overcome this drawback of conventional hydrogels, researchers are fabricating composite hydrogels with multi-scale structures, employing a reinforcement phase.[12] By incorporating multi-scale reinforcements, such as fabrics,[13,14] fibers,[15,16] and nanoparticles,[17,18] composite materials can be precisely engineered with tailored mechanical properties. These reinforcing phases utilize their distinct structural features and mechanical advantages to not only significantly improve the load-bearing capacity of the matrix through efficient stress transfer, but also introduce additional functionalities such as electrical conductivity and thermal responsiveness.[19–22] The reinforcement systems for hydrogel composites are primarily classified into three categories: fabric reinforced,[23,24] fiber reinforced,[25,26] and nanocomposite-reinforced.[27–29] Among these, fabric-reinforced composite hydrogels are typically fabricated by integrating hydrogels with fabric substrates, such as cotton, polyester, or aramid, *via* techniques including impregnation, coating, and *in situ* polymerization. In this design, the fabric framework is employed not only to provide mechanical stability to the hydrogel but also to impart novel functionality to the base textile.[30] Amber *et al.*[26] utilized a glass fiber fabric as an interlayer to achieve strong interfacial coupling between a polydimethylsiloxane (PDMS) elastomer and a polyzwitterionic hydrogel. This coupling is facilitated through mechanical interlocking and electrostatic interactions, resulting in a significant en-

* Corresponding author, E-mail: llwang@qdu.edu.cn
† These authors contributed equally to this work.
Received November 13, 2025; Accepted January 5, 2026; Published online February 6, 2026

hancement of mechanical properties and the successful realization of a synergistic rigid-flexible effect. However, fabric-reinforced composite hydrogels still suffer from weak interfacial adhesion between the matrix and the reinforcing phase. This weak bonding can lead to delamination or slippage under stress, significantly compromising the composite's overall strength. Fiber-reinforced composite hydrogels, which employ high-strength fibers as the reinforcing phase, can not only greatly enhance mechanical strength and fatigue resistance but also effectively preserve intrinsic properties such as flexibility and elasticity. Sun *et al.*[31] developed a multifunctional tendon-mimetic hydrogel (ACH) *via* a controllable assembly strategy based on aramid nanofiber (ANF) composites and poly(vinyl alcohol) (PVA). The ACH exhibited outstanding mechanical properties, achieving a fracture toughness reaching 98% of that of natural tendons, while maintaining excellent dimensional stability even under prolonged hydration. However, the modulus mismatch between rigid fibers and the soft matrix in fiber-reinforced hydrogels impedes a synergistic enhancement of strength and ductility. Nanoparticle-enhanced composite hydrogels are fabricated by incorporating nanoparticles into a hydrogel matrix, leveraging interfacial interactions between the nanoparticles and the polymer network to synergistically improve mechanical properties and impart multifunctionality. Arno *et al.*[32] developed morphologically tunable polymeric nanoparticles through crystallization-driven self-assembly (CDSA) and incorporated them into a calcium-alginate hydrogel matrix. This approach significantly enhanced the interfacial adhesion strength of the composite material, offering new strategies for the design of high-strength adhesive hydrogels. The high surface energy of nanoparticles poses a dual challenge: it readily induces particle agglomeration and triggers localized stress concentration, thereby critically compromising their efficacy as reinforcing phases. Based on the above discussion, the fabrication of hydrogel composites currently faces two major challenges. The first is weak interfacial bonding due to the mismatch between the reinforcing phase and the matrix, which prevents effective stress transfer to the reinforcement and thereby diminishes the reinforcing effect. Secondly, the modulus mismatch between the rigid reinforcement phase and the compliant matrix phase induces stress concentration at the interface, thereby limiting the overall improvement of the material's mechanical properties.

Herein, we present a novel composite hydrogel design strategy based on dynamic mechanical control, summarized as "blending reinforcement in the viscoelastoplastic state and fixing the structure in the viscoelastic state". This methodology leverages a unique PVA matrix capable of a thermally triggered viscoelastoplastic-to-viscoelastic transition. We demonstrate that this strategy not only effectively suppresses filler aggregation and reduces modulus mismatch but also achieves superior interfacial strength through structural reorganization. Consequently, the fabricated PVA/silica composite hydrogels exhibit outstanding mechanical properties, including enhanced crack-deflection capability and broadly tunable mechanics *via* a salt solution exchange strategy. This work thus provides a fundamental principle and a practical pathway for advancing the design of high-performance hydrogel composites.

## EXPERIMENTAL

### Materials

Poly(vinyl alcohol) (PVA, 1750, AR), anhydrous calcium chloride ($CaCl_2$, AR) were purchased from Sinopharm Chemical Reagent Co., Ltd. Nano-silica particles ($SiO_2$, 99%, rough aggregated diameters 15 nm/100 nm/300 nm/500 nm) were purchased from Shanghai Macklin Biochemical Co., Ltd. Deionized water was made by the laboratory. All aqueous solutions were prepared by deionized water.

### Preparation of High-density PVA/$SiO_2$ Composite Hydrogel

Initially, a homogeneous PVA/$CaCl_2$ mixed solution (20 wt% PVA, 2 mol/L $CaCl_2$) was prepared and allowed to swell statically for 12 h. The mixture was subsequently transferred to a 95 °C water bath and stirred continuously using a constant-speed electric stirrer at 300 r/min for 2 h until complete dissolution was achieved (Fig. S1a in the electronic supplementary information, ESI). The homogenized solution was then subjected to controlled dehydration in a 50 °C thermostatic environment for 8–12 h until a mass loss of approximately 37% was attained (Fig. S1b in ESI). Upon formation of a stretchable gel matrix, the material was transferred to a 70 °C heating stage where cyclic mechanical treatments (stretching, folding, and compression) were applied to incorporate $SiO_2$ at varying concentrations (0 wt%, 6 wt%, 12 wt%, and 18 wt%) (Fig. S1c in ESI). Finally, the composite hydrogel was molded, frozen at −20 °C for 12 h, and subsequently thawed at 27 °C, yielding a high-density PVA/$SiO_2$ composite hydrogel (Fig. S1d in ESI).

### Morphology Characterizations

The high-density PVA/$SiO_2$ composite hydrogel was treated in liquid nitrogen for 10 min before undergoing low-temperature brittle fracture to obtain intact cross-sectional morphology. The fractured samples were immediately transferred to a freeze dryer for continuous drying over 48 h. The dried specimens were subsequently sputter-coated with gold for 120 s using an ion sputtering coater. The prepared samples were then examined for surface microstructure characteristics using a scanning electron microscope (SEM, Hitachi S-4800) operated at an accelerating voltage of 20 kV. Elemental mapping of the surface was conducted using an X-ray energy-dispersive spectroscopy (EDS) system synchronized with the scanning electron microscope.

Surface morphological characterization of pre-notched specimens following mechanical loading was performed using a polarizing microscope (Axio Scope A1 POL) operated in bright-field mode.

### Spectroscopic Analyses

Fourier transform infrared (FTIR) spectroscopy analysis of the high-density PVA/$SiO_2$ composite hydrogel was conducted in attenuated total reflectance (ATR) mode with 32 scanning cycles at a resolution of 2 $cm^{-1}$. Structural characterization was performed across the wavenumber range of 4000–400 $cm^{-1}$.

### Mechanical Characterization

The tensile performance was evaluated using a tensile testing machine (WDW-2T), with the high-density PVA/$SiO_2$ composite hydrogel cut into 30 mm × 5 mm × 4 mm (length × width ×

thickness) rectangular sample strips, stretched at a rate of 50 mm/min. For the compression testing, cylindrical hydrogel specimens with dimensions of 10 mm in diameter and 8 mm in height were subjected to uniaxial compression at a constant crosshead speed of 10 mm/min until reaching 90% strain. Each sample measurements were conducted on at least five parallel samples, and the average value of the tensile performance was calculated.

Cyclic tensile and compressive tests were conducted using a universal testing machine. For the tensile cycling characterization, high-density PVA/$SiO_2$ composite hydrogel specimens were machined into rectangular strips measuring 30 mm × 5 mm × 4 mm (length × width × thickness). The tensile tests were performed at a constant crosshead speed of 50 mm/min following a multi-stage loading-unloading protocol: initial stretching to 100% strain with complete unloading, followed by successive loading-unloading cycles at incrementally increased strain levels of 200%, 300%, 400%, 500%, and 600%, ultimately reaching 700% strain for the final loading-unloading sequence.

Compression cycling tests employed cylindrical hydrogel specimens with dimensions of 10 mm diameter and 8 mm height was applied at a controlled rate of 10 mm/min through progressive loading-unloading cycles at 20%, 40%, 60%, and 80% compressive strain levels. The elastic recovery ratio ($R_e$), dissipated energy ($\Delta U$), and energy loss coefficient ($\eta$) of the composite hydrogel were quantitatively analyzed based on the hysteresis characteristics of both tensile and compressive cyclic curves, by using Eqs. (1)–(3).

$$R_e\ (\%) = \frac{\varepsilon_1 - \varepsilon_2}{\varepsilon_1 - \varepsilon_0} \times 100\% \tag{1}$$

$$\Delta U = \int_0^{\varepsilon_1} (\sigma_{load} - \sigma_{unload}) d\varepsilon \tag{2}$$

$$\eta = \frac{\Delta U}{\int_0^{\varepsilon_1} \sigma_{load} d\varepsilon} \times 100\% \tag{3}$$

where $\varepsilon_0$ is the strain of the sample with no external force, $\varepsilon_1$ is the strain of the sample after the external force is applied, and $\varepsilon_2$ is the residual strain of the sample after the external force is removed, $\sigma$ is the stress. $R_e$ is the ratio of the elastically recovered strain to the total applied strain after a complete loading-unloading cycle. $\Delta U$ is the area enclosed by the loading and unloading curves in a single loading–unloading cycle. $\eta$ is the ratio of the dissipated energy ($\Delta U$) to the total energy input during the loading process (the area under the loading curve).

## Notch Performance Measurements

Notched performance testing was conducted using tensile testing machine (WDW-2T). High-density PVA/$SiO_2$ composite hydrogels were fabricated into rectangular strips with dimensions of 30 mm × 45 mm × 4 mm (length × width × thickness). A 15 mm sharp pre-crack was introduced along the width direction through precision machining. Uniaxial tensile loading was applied at a constant crosshead speed of 50 mm/min. Five replicate tests were performed for both intact specimens and pre-cracked specimens, with the notch performance parameters calculated as mean values. Based on the tensile curves, three critical fracture parameters were determined: fracture work ($W$), fracture toughness ($\Gamma_T$), and critical cohesive zone length ($\varepsilon_T$).

## Swelling Measurements

High-density PVA/$SiO_2$ composite hydrogels with varying $SiO_2$ contents (0 wt%, 6 wt%, 12 wt%, 18 wt%) were molded into cylindrical specimens measuring 20 mm in diameter and 15 mm in height. Initial mass ($m_0$) and volume ($V_0$) were recorded prior to testing. The specimens were fully immersed in deionized water, with measurements conducted at 0.5 h intervals during the first 6 h, followed by 2 h intervals between 6 and 24 h, and finally extended to 24 h intervals beyond 24 h until swelling equilibrium was achieved. After each sampling, surface-adhered water was removed using dust-free filter paper before recording mass ($m_t$) and dimensional parameters ($V_t$). The mass variation ratio ($m_c$), volumetric variation ratio ($V_c$), and equilibrium swelling ratio (ESR) were subsequently calculated according to Eqs. (4)–(6).

$$m_c\ (\%) = \frac{m_t - m_0}{m_0} \times 100\% \tag{4}$$

$$V_c\ (\%) = \frac{V_t - V_0}{V_0} \times 100\% \tag{5}$$

$$ESR = \frac{m_s - m_0}{m_0} \times 100\% \tag{6}$$

where $m_t$ and $V_t$ denote the mass and volume of the composite hydrogel after swelling, respectively; $m_0$ and $V_0$ represent the initial mass and volume of the composite hydrogel prior to immersion; and $m_s$ corresponds to the equilibrium mass of the hydrogel at swelling completion. ESR refers to the percentage increase in the mass of a specimen relative to its initial value when its mass no longer shows a significant increase over time, indicating that swelling equilibrium has been reached.

## DSC Tests

The glass transition behavior of high-density PVA/$SiO_2$ composite hydrogel was investigated using differential scanning calorimetry (DSC 250). Freeze-dried samples weighing 10 mg were precisely loaded into hermetically sealed aluminum pans. The temperature protocol comprised sequential stages: initial heating from ambient conditions to 250 °C at a rate of 50 °C/min, followed by a 3 min isothermal hold. Subsequent cooling to 10 °C at 50 °C/min preceded a 3 min stabilization period, after which the samples were reheated to 250 °C at the identical heating rate. The heating and cooling curves of the process were recorded.

## TGA Tests

The water content of high-density PVA/$SiO_2$ composite hydrogel was assessed by a thermogravimetric analyzer (SDT650). High-density PVA/$SiO_2$ composite hydrogel with weight of about 8 mg were introduced to the alumina crucibles. The samples were ramped up to 300 °C at 5 °C/min.

## ICP Tests

The calcium ion content in high-density PVA/$SiO_2$ composite hydrogel was quantitatively analyzed using inductively coupled plasma optical emission spectrometry (ICP-OES). Approximately 1 g of sample was accurately weighed and transferred into a 1 L volumetric flask. The sample was dissolved in deionized water via ultrasonic-assisted method, followed by dilution to the volumetric mark. The calcium ion concentration was determined through ICP-OES measurement, and the original content in the gel was calculated using the dilution factor.

https://doi.org/10.1007/s10118-025-3547-8

### Finite Element Analysis Simulations

Finite element analysis (FEA) was conducted using commercial ABAQUS software (version 2022, Simulia, Providence) to evaluate the crack resistance of pre-cracked PVA hydrogels and high-density PVA/$SiO_2$ composite hydrogel specimens. The constitutive parameters were defined as follows: Young's modulus ($E$) of 90 GPa with Poisson's ratio ($v$) of 0.2 for $SiO_2$, and 1.13 MPa ($E$) with 0.4 ($v$) for the PVA hydrogel matrix, corresponding to their respective material phases in the simulation.

## RESULTS AND DISCUSSION

### Design Principle of Composite Hydrogel Based on Dynamic Mechanics

Based on a novel viscoelastoplastic PVA physical hydrogel previously developed by our group, this study presents an innovative strategy and fundamental principle for fabricating composite hydrogel, namely, "blending fillers in the viscoelastoplastic state and fixing the structure in the viscoelastic state". The viscoelastoplastic hydrogel exhibits notable moldability and shape retention after large deformation, rather than flowing like a liquid sol state. It can be extensively stretched and reshaped instantly (Video S1 in ESI), which is characteristic of the unique viscoelastoplastic state designed in this work. Under moderate thermal conditions, the hydrogel exhibits a viscoelastoplastic state that allows for the effective dispersion of incorporated phases through cyclical mechanical processing. Subsequent cooling induces a transition to a viscoelastic state, enabling structural fixation of the composite hydrogel. The design concept is schematically depicted in Fig. 1. The proposed methodology begins with a novel viscoelastoplastic PVA hydrogel matrix featuring an amorphous/strong hydrogen-bonding hierarchical architecture with complementary weak/strong interactions. This unique design utilizes moderate-strength hydrogen bonds to enable rapid shape fixation without compromising matrix deformability. Concurrently, the amorphous polymer network promotes conformational adjustments of the polymer chains, which accelerates the dynamic exchange ("association-disassociation") kinetics of hydrogen bond and improves the ductility of the hydrogel. These mechanisms collectively contribute to the viscoelastoplastic behavior of physical PVA hydrogel. Furthermore, leveraging the mechanical transition of this hydrogel system from a high-temperature viscoelastoplastic state to a low-temperature viscoelastic state, we developed a novel processing strategy that involves "mixing fillers in the viscoelastoplastic state (Fig. 1a) and fixing the structure in the viscoelastic state (Fig. 1c)". This innovative strategy enabled the successful development of high-strength, tough PVA/$SiO_2$ composite hydrogels with outstanding mechanical properties. (1) During the high-temperature viscoelastoplastic state, a mechanical mixing process involving multiple folding-compression cycles was employed. This method not only promoted the alignment of polymer chains but also significantly improved the uniform dispersion of nanoparticles and their filling capacity within the hydrogel matrix (Fig. 1b). (2) Subsequent freeze-thaw cycles induced phase separation of polymer and a further reorganization of hydrogen bonding between PVA chains, leading to the dimensional stabilization and structural fixation of the

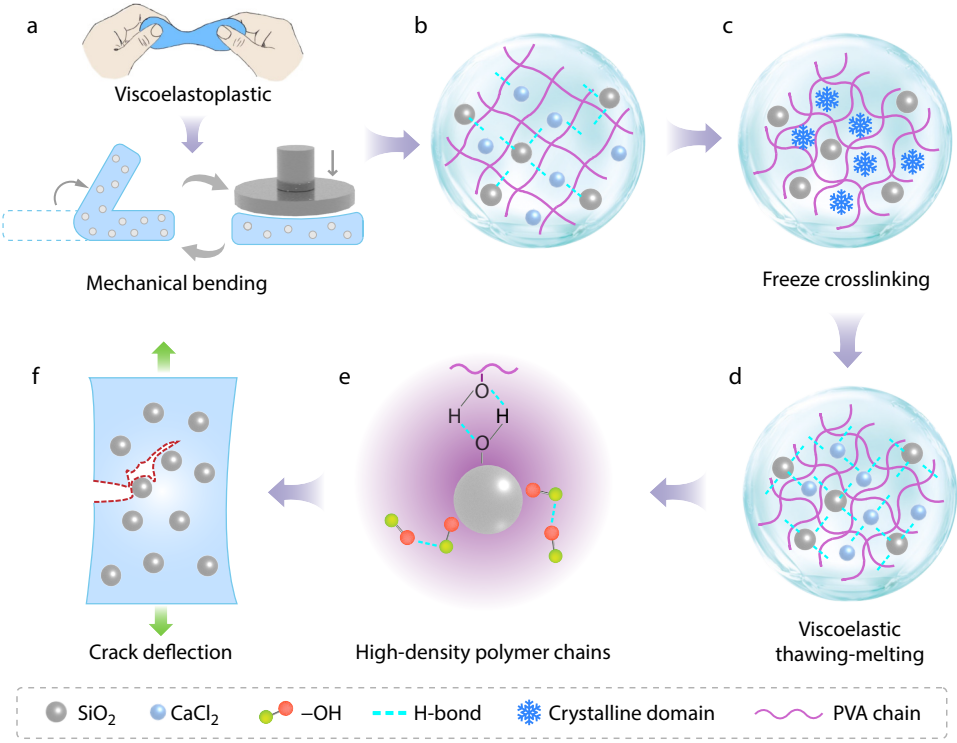


**Fig. 1** (a) Mechanical compounding of $SiO_2$ into a viscoelastoplastic PVA hydrogel; (b) Schematic molecular structure of the highly-density PVA/$SiO_2$ composite hydrogel; (c, d) Freeze-thaw cycling process of the PVA/$SiO_2$ composite hydrogel; (e) Formation mechanism of strong interfacial hydrogen bonds; (f) Illustrative depiction of crack-deflecting and blunting mechanisms in composite hydrogel within high-loading fillers.

https://doi.org/10.1007/s10118-025-3547-8

composite hydrogel (Figs. 1c and 1d). The proposed method offers significant advantages: (1) Mechanical compounding carried out in a high-temperature viscoelastoplastic state effectively reduces the typical filler aggregation observed in conventional solution-based compounding techniques, thereby greatly expanding the blending phases available for hydrogel composites. (2) The inherently highly dense polymer chains and numerous hydrogen bonding in the viscoelastoplastic hydrogel (Fig. 1e) markedly reduce the modulus mismatch between the hydrogel and the dispersed phases, thereby effectively addressing the long-standing challenge of weak interfacial adhesion caused by high modulus mismatch in composite hydrogel systems. (3) The superior interfacial strength arises from three key factors: the inherent abundance of physical interactions among the high-density polymer chains in the viscoelastoplastic hydrogel, the physical bonding between polymer chains and $SiO_2$ microspheres (Fig. 1e), and the secondary reorganization of physical interactions during viscoelastic molding. Based on the aforementioned advantageous structural features, the strong interfacial bonding between $SiO_2$ particles and the matrix is expected to lead to localized stress concentration when external loads cause propagating cracks to approach the particulate regions. This interfacial interaction promotes crack front deflection, causing a deviation from linear propagation to bent or tortuous paths. The observed flexural behavior facilitates efficient energy dissipation and improves crack-propagation resistance (Fig. 1f). This composite material shows promise for mechanical protective applications like artificial cartilage, where controlled energy absorption and crack resistance are critical.

## Mechanical Properties of High-density PVA/$SiO_2$ Composite Hydrogel

This study presents a systematic investigation of how nanofiller content and particle size influence the mechanical properties of composite hydrogels (Fig. 2). According to the stress-strain curves of PVA composite hydrogels with varying silica particle sizes and contents (Fig. 2a and Fig. S2 in ESI), both the Young's modulus ($E$) and fracture strength ($\sigma_f$) increase significantly with increasing $SiO_2$ particle size and content. The composite exhibits optimal mechanical performance at a 500 nm $SiO_2$ loading of 18 wt%, achieving a fracture strength ($\sigma_f$) of 2.12 MPa and a Young's modulus ($E$) of 0.84 MPa. The composites demonstrated optimal mechanical properties at a $SiO_2$ loading of 18 wt%, achieving a fracture strength ($\sigma_f$) of 2.12 MPa and a Young's modulus ($E$) of 0.84 MPa. In terms of compressive performance (Figs. 2b, 2d and 2f), the composite hydrogels show a marked improvement in both compressive strength and modulus as the $SiO_2$ content increases. At the optimal concentration, the hydrogel composite reached a maximum compressive strength of 15.2 MPa, with a corresponding modulus of 1.32 MPa. Furthermore, regarding the effect of $SiO_2$ particle size on the mechanical properties of PVA composite hydrogels (Figs. 2d and 2f, Figs. S3a–S3c in ESI), at a fixed filler content ($C_{SiO_2}$=18 wt%), the compressive strength of the composites increased markedly from 9.75 MPa to 15.2 MPa, while the compressive modulus rose from 0.57 MPa to 1.23 MPa, as the $SiO_2$ particle size increased from 15 nm to 500 nm. A contributing factor is the distinctive flexural toughening mechanism exhibited by larger-size particles. Specifically, under compressive loading, the 500 nm $SiO_2$ particles exhibit enhanced elastic flexural deformation. This mechanism efficiently absorbs energy and subsequently delays the propagation of cracks within the matrix. Additionally, larger-diameter silica microspheres benefit from the unique processing conditions of composite hydrogels, achieving excellent dispersion during mechanical compounding in the viscoelastoplastic state and thus exhibiting a higher reinforcing efficiency in the composite.

Moreover, the markedly enhanced energy dissipation of the composite hydrogel underpins its superior toughness. As evidenced by the cyclic tensile loading-unloading curves (Fig. 2g, Figs. S4 and S5 in ESI), the dissipated energy ($\Delta U$) is calculated as the area enclosed by the hysteresis loops. Meanwhile, the energy dissipation coefficient ($\eta$) is defined to quantify the material's energy dissipation efficiency under cyclic loading conditions (Fig. 2h). The composite hydrogel incorporated with 500-nm $SiO_2$ particles ($C_{SiO_2}$=18 wt%) exhibited markedly improved energy dissipation properties compared to the pure PVA hydrogel, with $\Delta U$ and $\eta$ values measured to be 9.62 and 1.57 times higher than those of the pristine matrix, respectively. Notably, the toughness of the material increases approximately linearly with the $C_{SiO_2}$ content rising from 0 wt% to 18 wt%, reaching a maximum value of 4.18 MJ/m$^3$ (Fig. 2i). In summary, the dynamic mechanics-based composite processing strategy leads to a simultaneous enhancement in both the strength and toughness of the hydrogel, resulting in superior mechanical performance. Moreover, broad tunability in mechanical properties is enabled through precise modulation of the $SiO_2$ content and particle size. Under a 25 N applied load, composite hydrogel strips (80 mm × 5 mm × 4 mm) exhibited no structural failure, confirming their mechanical integrity (Fig. 2e).

The mechanical reinforcement exhibited by this composite hydrogel stems from three key contributions. Firstly, the viscoelastoplastic hydrogel matrix possesses a higher intrinsic polymer chain density than conventional hydrogels, leading to a significant reduction in the modulus mismatch between the matrix and the dispersed phase. This synergistic effect ensures a more uniform stress distribution while overcoming the interfacial incompatibility issues that commonly arise from large modulus differences in heterogeneous materials. Secondly, robust interfacial adhesion is established through strong hydrogen bonding between PVA chains and $SiO_2$ surfaces.[33] This adhesion is critical for enabling efficient stress transfer to the reinforcing phases. The hydrogel matrix facilitates the formation of a cohesive network architecture from dispersed reinforcing phases. This dual mechanism serves to mitigate localized stress concentrations under load while simultaneously enabling energy dissipation through controlled structural reorganization, thereby establishing the fundamental physical basis for creating hydrogels with exceptional toughness and crack resistance. Third, the introduction of $SiO_2$ fundamentally transforms the nature of crack propagation, replacing simple linear advancement with complex, nonlinear trajectories. This transition leads to a marked improvement in energy dissipation efficiency.

## Crack Propagation Resistance of High-density PVA/$SiO_2$ Composite Hydrogel

Crack insensitivity serves as a key indicator for evaluating a material's resistance to fracture, playing an essential role in guaran-

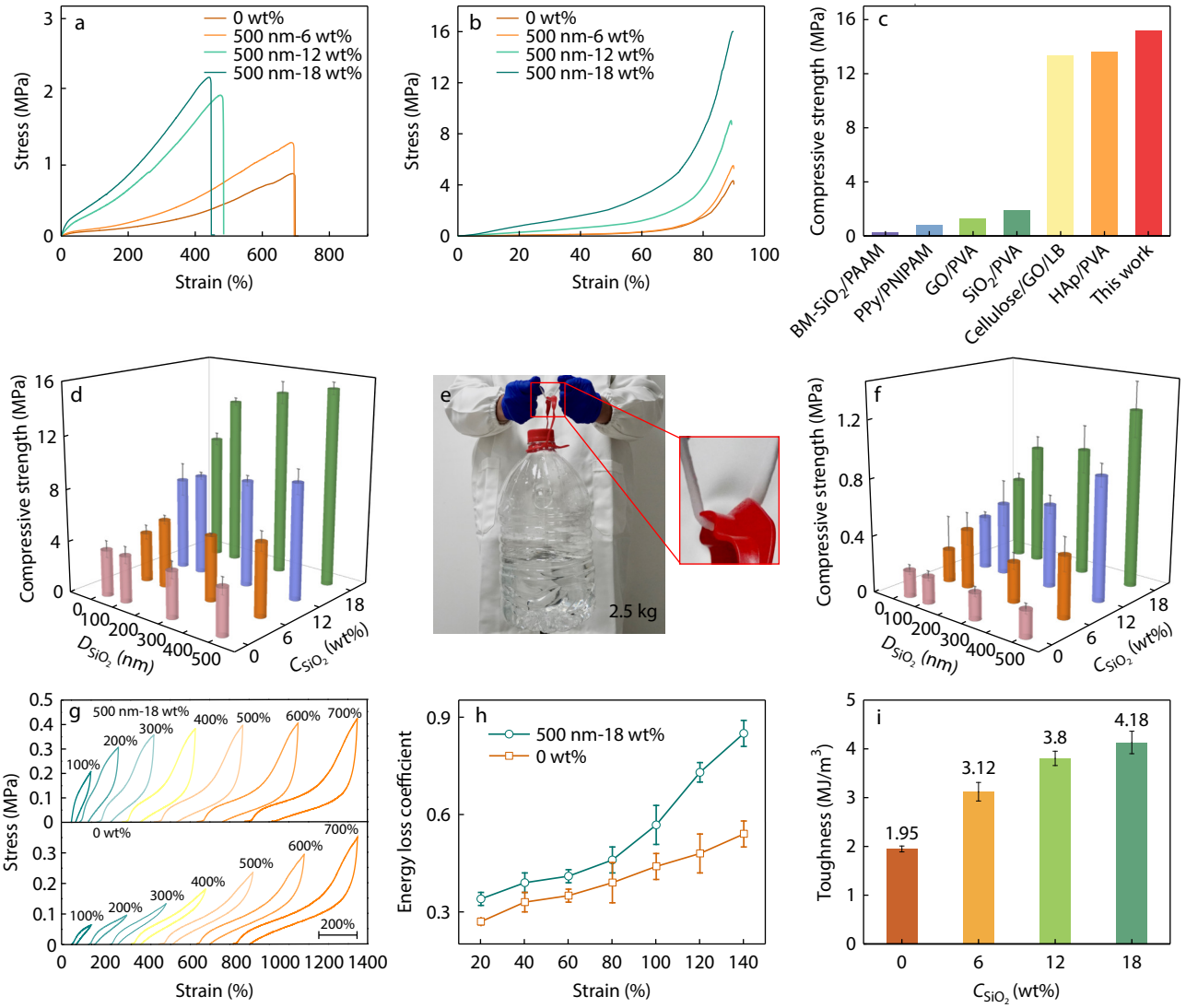


**Fig. 2** (a) Variation of tensile curves of high-density PVA/$SiO_2$ composite hydrogel with $SiO_2$ content; (b) Variation of compression curves of high-density PVA/$SiO_2$ composite hydrogel with $SiO_2$ content; (c) Comparison of compressive strength between high-density PVA/$SiO_2$ composite hydrogel and other hydrogels; (d) Variation of compressive strength of high-density PVA/$SiO_2$ composite hydrogel with $SiO_2$ content and size; (e) Load-bearing capacity of a composite hydrogel strip with dimensions of 80 mm × 5 mm × 4 mm (length × width × thickness); (f) Variation of compressive modulus of high-density PVA/$SiO_2$ composite hydrogel with $SiO_2$ content and size; (g) Tensile cyclic curves (0%–100%) of PVA hydrogel and high-density PVA/$SiO_2$ composite hydrogel; (h) Energy loss coefficient of PVA hydrogel and high-density PVA/$SiO_2$ composite hydrogel; (i) Variation of toughness with silica content in high-density PVA/$SiO_2$ composite hydrogel.

teeing structural reliability under complex loading conditions and long-term operation. This study systematically investigated the crack propagation resistance of PVA/$SiO_2$ composite hydrogels.

Based on the stress-strain curves of unnotched and notched composite hydrogels (Fig. 3a), as the $SiO_2$ content increased from 0 wt% to 18 wt%, the notched-to-unnotched ratio of fracture strength increased from 0.41 to 0.75, the ratio of elongation at break rose from 0.50 to 0.71, and the ratio of fracture toughness grew from 0.13 to 0.56. Compared to pure PVA hydrogels, the composite hydrogel (500 nm, 18 wt%) exhibited significant enhancements in mechanical properties, with increases by a factor of 1.8 in fracture strength, 1.4 in fracture elongation, and 4.3 in fracture toughness, demonstrating outstanding resistance to crack propagation. To further advance the understanding of resistance to crack propagation, this study introduces the fracture cohesive length ($\varepsilon_T$, Eqs. 7–9) as a quantitative metric. Here, $\Gamma_T$ represents the fracture toughness of the notched hydrogel, and $W$ denotes the fracture work of the unnotched hydrogel. The parameter $\varepsilon_T$ can be used to assess the spatial extent of energy dissipation during fracture. The results indicated that with increasing $SiO_2$ content, the fracture cohesive length of the composite hydrogel increased from 3.71 mm to 8.16 mm (Fig. 3b). This suggests that a higher $SiO_2$ content significantly prolonged the crack propagation path, thereby effectively reducing the notch sensitivity and enhancing the crack propagation resistance of the hydrogel. Meanwhile, the fracture cohesive length, as indicated by the slope of the $\Gamma_T$-$W$ plot, reveals distinct energy dissipation behaviors across various soft materi-

https://doi.org/10.1007/s10118-025-3547-8

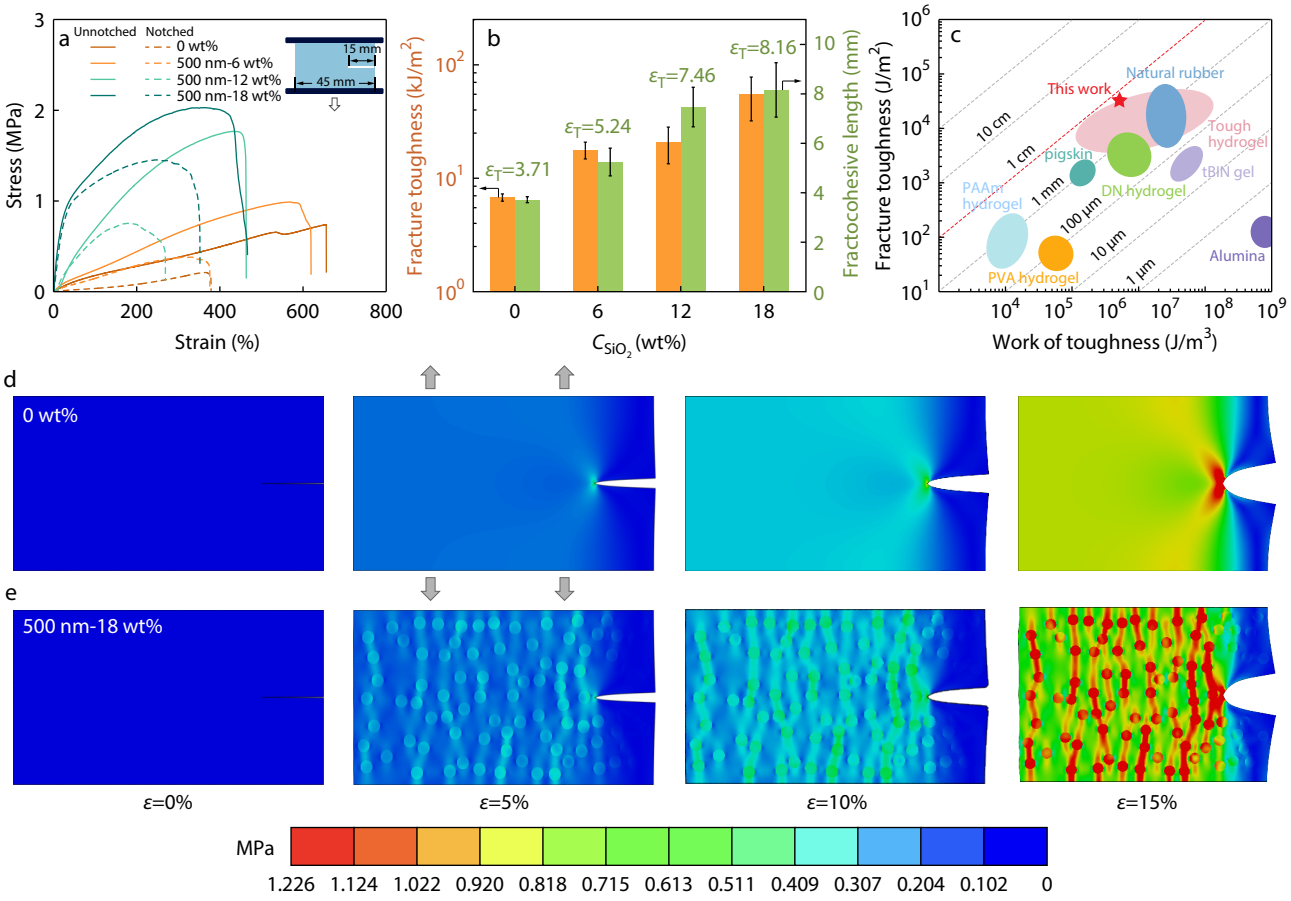


**Fig. 3** (a) Stress-strain behavior of unnotched and pre-notched high-density PVA/$SiO_2$ composite hydrogels; (b) Fracture toughness and fracture cohesive length of high-density PVA/$SiO_2$ composite hydrogels versus silica content; (c) Comparative investigation of the cohesive fracture length in flexible materials; (d, e) Finite element analysis of the stress distributions in pure PVA and high-density PVA/$SiO_2$ composite hydrogels under different strains.

als (Fig. 3c). The high-density PVA/$SiO_2$ composite hydrogel demonstrated superior energy dissipation capability, significantly surpassing that of double-network hydrogels and PAAM hydrogels, and performing comparably to tough hydrogels.

$$W = \int_0^{\varepsilon_1} \sigma_{\text{load}} \mathrm{d}\varepsilon \tag{7}$$

$$\Gamma_{\text{T}} = \int_0^{\varepsilon_{n1}} \sigma_{\text{load}} \mathrm{d}\varepsilon_n \times h \tag{8}$$

$$\varepsilon_{\text{T}} = \frac{\Gamma_{\text{T}}}{W} \tag{9}$$

where $\sigma$ is the tensile stress of the intact specimen, $\varepsilon_1$ denotes the strain of the intact specimen under applied load, $\varepsilon_n$ denotes the strain of the pre-cracked specimen, $\varepsilon_{n1}$ corresponds to the strain of the pre-cracked specimen under applied load, and $h$ is the initial gauge length between the two grips.

To elucidate the unique crack passivation mechanism of the composite system, we performed finite element simulations comparing neat PVA hydrogel with the high-density PVA/$SiO_2$ composite hydrogel (Figs. 3d and 3e). Finite element simulations reveal that the neat PVA hydrogel develops a stress concentration at the notch tip during the initial loading stage ($\varepsilon$=5%). Upon reaching a strain of 10%, a symmetric biconical stress distribution is observed to form at the notch tip. When the strain reaches 15%, the equivalent stress contour plot forms a distinct butterfly pattern. This is accompanied by significant stress concentration, which triggers unstable crack propagation. Compared to other formulations, the high-density PVA/$SiO_2$ composite hydrogel exhibits a significantly more uniform stress distribution under small strains. When the strain reached 15%, although local stress concentration emerged at the crack tip, the principal stresses remained largely confined to the silica particles and were transmitted along their paths. This mechanism facilitated energy dissipation and helped mitigate brittle fracture of the material. Further *in situ* morphological analysis of pre-notched specimens (Fig. S6 in ESI) reveals a marked difference in fracture behavior between neat PVA and high-density PVA/$SiO_2$ composite hydrogels: as the strain increases, the fracture surface of pure PVA remains smooth, exhibiting rapid, straight crack propagation characteristic of typical brittle fracture; whereas with increasing $SiO_2$ content, the composite hydrogel shows obvious crack-tip blunting, path deflection, and branching. This visible transition from sharp to blunted cracks directly demonstrates that the incorporation of $SiO_2$ expands the fracture process zone and enhances the material's resistance to crack propagation. The energy dissipation in the high-density

https://doi.org/10.1007/s10118-025-3547-8

PVA/$SiO_2$ composite hydrogel originates from its multi-scale structure, which enables efficient energy dissipation through several synergistic mechanisms. The underlying mechanism originates from three key factors. Firstly, the high-density polymer chains constructed by the viscoelastoplastic hydrogel provides an abundance of dynamic physical cross-linking points. Secondly, strong interfacial bonding is established between the polymer chains and the $SiO_2$ microspheres *via* hydrogen bonding. Finally, the dynamic reorganization process of the physical cross-linking network during freezing treatment leads to an optimized interfacial structure. When a crack approaches a silica particle, the strong interface between the particle and the matrix induces local stress concentration, leading to deflection of the crack front. This process endows the high-density PVA/$SiO_2$ composite hydrogel with superb resistance to crack propagation.

Based on the above crack propagation resistance mechanism, the composite hydrogel exhibits excellent puncture resistance (Fig. S7 in ESI). The results indicate that as the silica content increases from 0 wt% to 18 wt%, the puncture strength of the composite hydrogel is significantly enhanced, with the puncture force rising from 0.17 N to 2.93 N and the corresponding puncture energy jumping from 7.98 MJ to 20.52 MJ. Observation of the macroscopic morphology (inset in Fig. S7 in ESI) during puncture reveals a characteristic umbrella-shaped distribution of stress within the composite hydrogel. The synergistic interaction between silica and PVA chains facilitates an energy dissipation mechanism, which effectively inhibits crack propagation. This high-density composite structure imparts exceptional puncture resistance.

Based on the above, the high-density PVA/$SiO_2$ composite hydrogel significantly suppresses crack propagation due to its densely cross-linked polymeric network and strongly embedded $SiO_2$ structure, demonstrating exceptional performance as a mechanical protective material.

## Broad-range Tunability of Mechanical Properties in High-density PVA/$SiO_2$ Composite Hydrogels

The structural features of the composite hydrogels, such as their high calcium ion content and moderate water content, enable the wide-range tuning of their mechanical properties *via* the solvent exchange method. Based on this, the present study proposes a strategy for the secondary tuning of the mechanical properties of high-density PVA/$SiO_2$ composite hydrogels by employing $CaCl_2$ solutions at varying concentrations (0, 2, 4, 6, and 8 mol/L).

The water exchange behavior of the high-density PVA/$SiO_2$ composite hydrogel in deionized water was first investigated. Based on the mass changes of composites with varying $SiO_2$ content (Fig. S8a in ESI), all samples exhibit characteristic two-stage swelling behavior. During the initial stage (0–70 h), the mass change rate of the samples increases rapidly. In the second stage (70–120 h), the rate of mass gain gradually tapers off, reaching an equilibrium swelling state after approximately 120 h. It is noteworthy that as the $SiO_2$ content increased from 0 wt% to 18 wt%, the equilibrium swelling ratio (ESR) of the composite hydrogel decreased significantly from 188.27% to 156.88%. These results indicate that the $SiO_2$ content markedly influences the swelling behavior of the hydrogel, and that the nanoparticles effectively suppress swelling-induced dimensional instability. Similarly, analysis of the volume changes in the nano-composite hydrogel with 500 nm particle size (Figs. S8b and S8c in ESI) reveals that composites containing 18 wt% $SiO_2$ exhibits superior dimensional stability. Moreover, larger $SiO_2$ nanoparticles were more effective in enhancing the anti-swelling properties of the composite hydrogel, which aligns with the trends observed in their mechanical performance. The anti-swelling performance of nanocomposite hydrogels is primarily attributed to two key factors. First, the high-density polymer chains within the viscoelastic hydrogel form numerous physical hydrogen bonds, leading to a greater density of physical cross-linking sites compared to conventional hydrogels. Secondly, the physical interactions between the high-density polymer chains and the $SiO_2$ microspheres establish a robust interfacial structure, which significantly enhances the overall mechanical integrity and stability of the composites. Furthermore, the freezing-induced phase separation of polymer further reinforces the entire physical cross-linking network. These two factors work together to significantly limit swelling and structural degradation in water, giving the composite hydrogel exceptional dimensional stability.

It is particularly notable that the composite hydrogel exhibits pronounced changes in its mechanical properties after attaining swelling equilibrium in deionized water (Fig. 4a and Fig. S9 in ESI). Compared to its non-swollen state, the deionized water-swollen high-density PVA/$SiO_2$ composite hydrogel (500 nm, 18 wt%) exhibited a decrease in tensile strength from 2.12 MPa to 1.31 MPa, a reduction in Young's modulus from 0.84 MPa to 0.19 MPa, and a decline in compressive strength from 15.2 MPa to 9.89 MPa. These changes indicate a significant rigid-to-flexible transition in the mechanical behavior of the hydrogel upon water absorption. It is noteworthy that the swollen high-density PVA/$SiO_2$ composite hydrogel demonstrates markedly improved resilience under both tensile and compressive loading (Figs. 4b and 4c and Figs. S10–S12 in ESI). According to the cyclic tensile tests, the unloading curve of the swollen composite hydrogel (500 nm, 18 wt%) almost completely coincides with the loading curve (Fig. S10 in ESI), whereas a significant hysteresis loop is observed in the composite hydrogel prior to swelling. Compared to the original composite hydrogel, the swollen counterpart exhibits a 48.6% reduction in dissipated energy under a pre-strain of $\varepsilon$=100%. This improvement is further underscored by the compressive resilience measurements, which highlight the significant role of swelling in enhancing the dynamic recovery behavior of the hydrogel. The swollen composite hydrogel (500 nm, 18 wt%) exhibits an elastic recovery rate of 63.88% under 80% compressive strain (pre-stretching strain $\varepsilon$=80%), representing a 5.4-fold increase compared to the unswollen sample. Through swelling equilibrium treatment, the resilience of the composite hydrogel is notably enhanced, yielding a superior balance of strength, toughness, and elasticity.

Furthermore, the mechanical properties of high-density PVA/$SiO_2$ composite hydrogels were effectively modulated by varying the $CaCl_2$ concentration in the swelling solution. First, when the $CaCl_2$ concentration was varied from 0 mol/L to 4 mol/L, the composite hydrogels exhibit water absorption and

https://doi.org/10.1007/s10118-025-3547-8

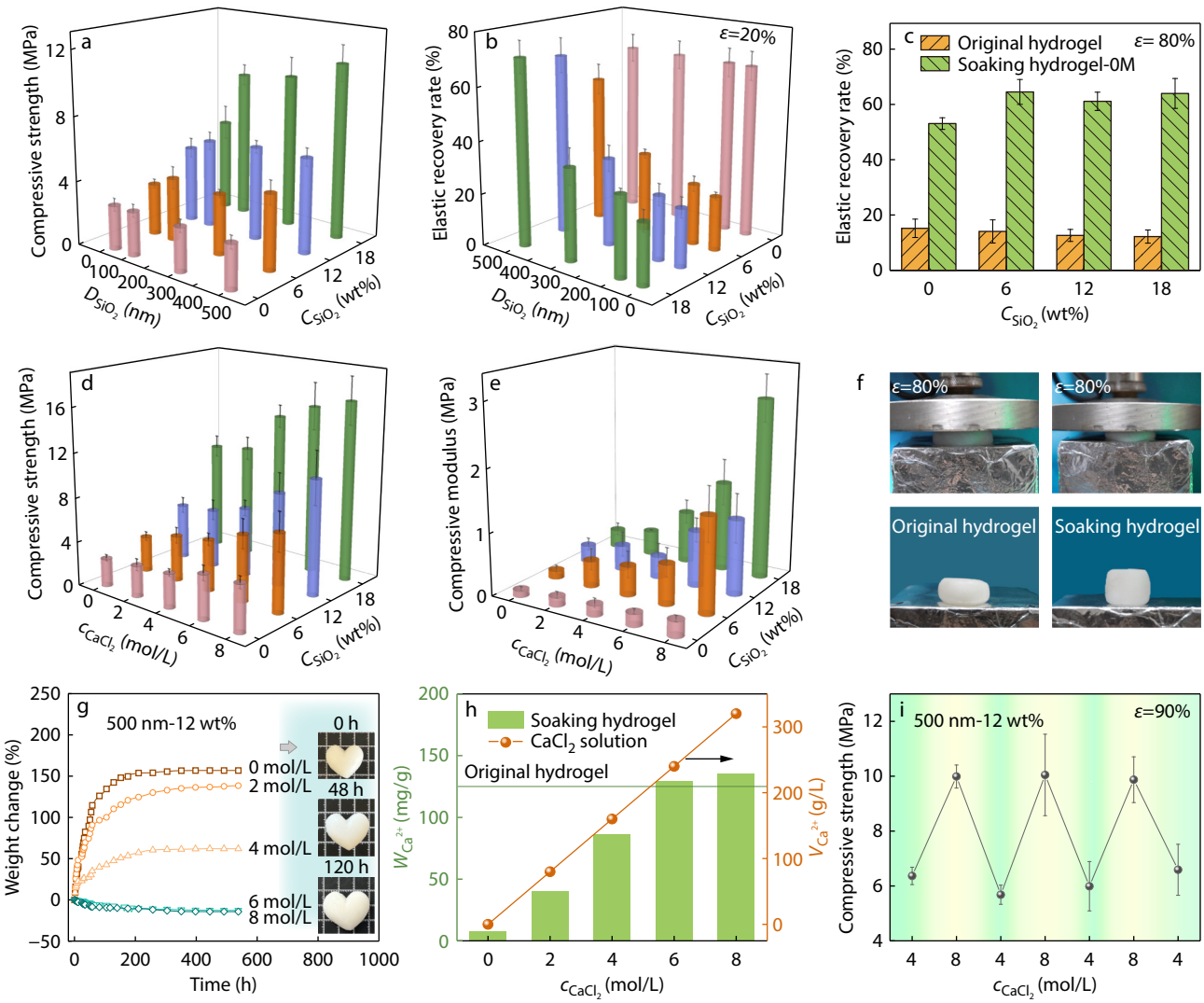


**Fig. 4** (a, b) The compressive strength and elastic recovery of composite hydrogels at swelling equilibrium (in deionized water) as a function of $SiO_2$ content and particle size; (c) Variation in the elastic recovery rate of composite hydrogels (after versus before swelling in deionized water) with $SiO_2$ content; (d, e) Effects of $SiO_2$ content and swelling salt concentration on the compressive strength and modulus of composite hydrogels; (f) The resilience of the PVA/$SiO_2$ composite hydrogels was compared by applying a compressive force (*e.g.*, by stepping) before and after swelling; (g) Mass change kinetics of the 500 nm, 12 wt% composite hydrogel in $CaCl_2$ solutions of varying concentrations (the inset shows macroscopic images of the hydrogel swollen in deionized water at 0, 48, and 120 h); (h) A comparison among the swelled 500 nm, 12 wt% composite hydrogel in $CaCl_2$ solutions of varying concentrations, the original un-swelled hydrogel, and the corresponding $Ca^{2+}$ content variation in the solutions; (i) The compressive strength of the 500 nm, 12 wt% composite hydrogel was measured after cyclic swelling treatments in 4 and 8 mol/L $CaCl_2$ solutions.

volumetric swelling over 23 days (Fig. 4g and Fig. S13 in ESI). As the $CaCl_2$ concentration increased, the rate of mass change in the composite hydrogels progressively decreased. When the concentration of $CaCl_2$ exceeds 6 mol/L, the composite hydrogel displays dehydration behavior, resulting in a macroscopic contraction. Therefore, the composite hydrogel exhibits a stable equilibrium in $CaCl_2$ solutions at concentrations between 4 and 6 mol/L. Furthermore, the $Ca^{2+}$ content of the composite hydrogel was quantified using inductively coupled plasma spectroscopy (ICP) (Fig. 4h). The results indicate that the $Ca^{2+}$ concentration within the swollen hydrogel increased correspondingly with higher concentrations of $CaCl_2$ in the swelling solution. However, compared to the inherent $Ca^{2+}$ level of the original hydrogel (as indicated by the green line in Fig. 4h), swelling in $CaCl_2$ solutions with concentrations ranging from 0 mol/L to 4 mol/L led to a decrease in $Ca^{2+}$ concentration within the hydrogel, while the hydrogel exhibits water absorption behavior. When the concentration of $CaCl_2$ in the swelling medium is in the range of 6–8 mol/L, the $Ca^{2+}$ concentration increases following the swelling of the composite hydrogel, accompanied by a dehydration behavior of the hydrogel. Regarding the mechanical properties of the swollen composite hydrogel, both the compressive strength and compressive modulus of the high-density PVA/$SiO_2$ composite hydrogel increase significantly with the concentration of the $CaCl_2$ swelling solution (Figs. 4d and 4e). For example, upon reaching swelling equilibrium in deionized water, the compressive strength and compressive modu-

https://doi.org/10.1007/s10118-025-3547-8

lus of the composite hydrogel were determined to be 9.89 and 0.19 MPa, respectively. When the $CaCl_2$ solution concentration used for swelling was increased to 8 mol/L, both the compressive strength and compressive modulus increased, reaching values of 16.29 and 2.13 MPa, respectively. Additionally, when subjected to cyclic changes in salt concentration (alternating between 4 and 8 mol/L $CaCl_2$ solutions), the composite hydrogel retained 95% of its initial mechanical strength after three swelling-deswelling cycles. Its mechanical properties exhibited reversible, concentration-dependent behavior. The mechanical properties of the composite hydrogel can be dramatically altered using salt solutions, allowing them to be tailored for a broad spectrum of load-bearing applications.

In summary, the mechanical properties of composite hydrogels can be reversibly and broadly modulated by a salt solution exchange strategy, achieved primarily by adjusting the following structural mechanisms. The robust hydrogen bonding at the interface between the high-density polymer chains and the $SiO_2$ microspheres confers upon the composite both dynamically stable interfacial binding and tunable swelling characteristics. At low salt concentrations, the high $CaCl_2$ content in the composite hydrogel promotes water absorption. During swelling, water molecules penetrate the interchain spaces, resulting in enhanced polymer chain mobility. This network structure is stabilized by robust polymer-nanoparticle interfaces, which function as physical cross-linking points. As a result, the composite hydrogel demonstrates superior resilience following water absorption. However, when the salt concentration surpasses the intrinsic ion concentration of the composite hydrogel, dehydration occurs. This process increases the density of polymer chains and nanoparticles per unit cross-sectional area, accompanied by augmented overall physical interactions. The consequent reinforcement of these interactions significantly enhances the mechanical strength of the hydrogel.

## Microstructure of High-density PVA/$SiO_2$ Composite Hydrogel

To elucidate the structural mechanism of composite hydrogels, we systematically investigate the multi-scale microstructure of high-density PVA/$SiO_2$ composite hydrogel (Fig. 5). Scanning electron microscopy (SEM) demonstrates the uniform dispersion of nano-$SiO_2$ particles throughout the PVA matrix in the high-density PVA/$SiO_2$ composite hydrogel. A progressive increase in nano-$SiO_2$ content correlates with a higher density of surface particles, leading to a coarser morphology and enhanced prominence of granular structures in the composite hydrogel (Figs. 5a–5d). Higher magnification reveals distinct changes in the granular structure and an increase in particle density (Figs. 5e–5h). Cross-sectional morphology and EDS elemental analysis of Si reveal a relatively uniform distribution of nanoparticles within the hydrogel matrix (Fig. S14 in ESI).

Furthermore, the FTIR spectra of nano-silica composite hydrogels with different particle sizes at maximum filler content (Fig. 5i) reveal a distinct absorption band at 3350 $cm^{-1}$ in all samples, corresponding to the stretching vibration of hydrox-

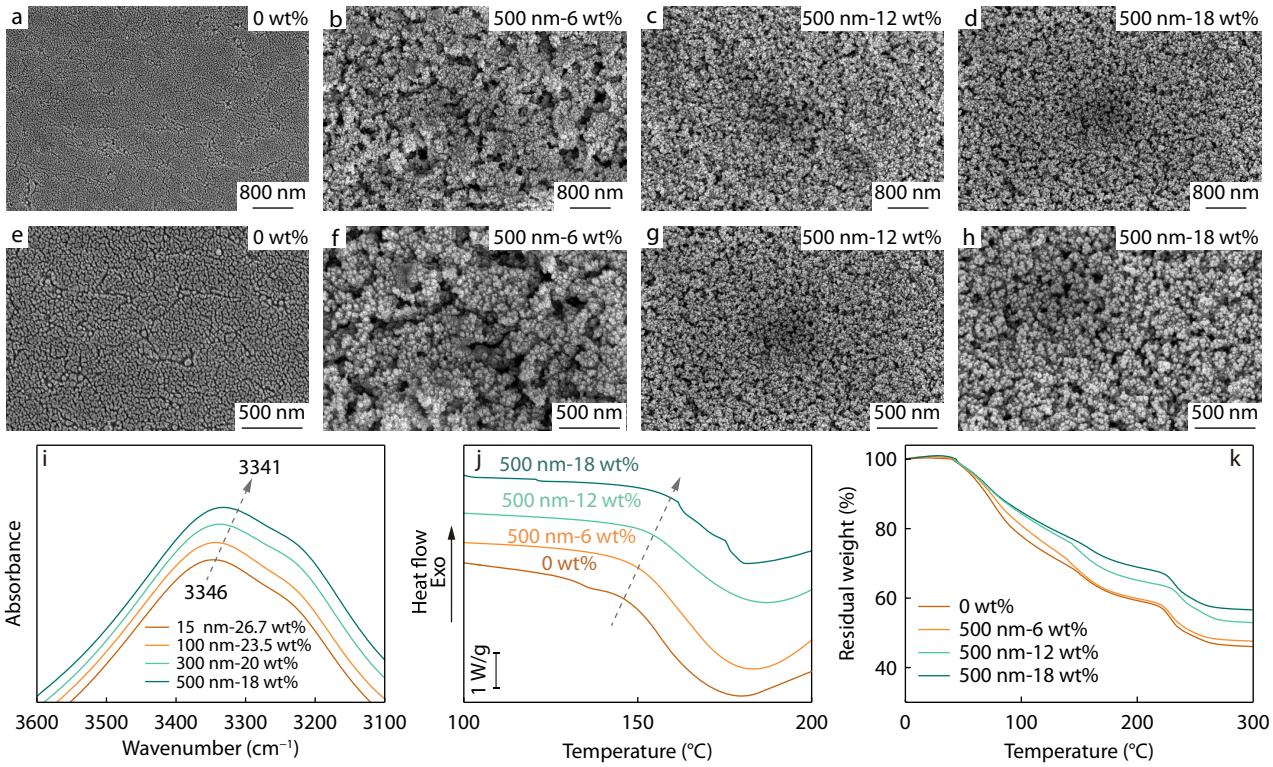


**Fig. 5** (a–h) SEM images of high-density PVA/$SiO_2$ composite hydrogels with varying $SiO_2$ contents; (i) FTIR spectra in the 3600–3100 $cm^{-1}$ region for high-density PVA/$SiO_2$ composite hydrogels containing the maximum filler content, with varying $SiO_2$ particle sizes; (j) DSC thermograms of high-density PVA/$SiO_2$ composite hydrogels with varying $SiO_2$ contents; (k) TGA thermograms depicting the thermal degradation of high-density PVA/$SiO_2$ composite hydrogels with varying $SiO_2$ contents.

https://doi.org/10.1007/s10118-025-3547-8

yl groups in the PVA hydrogel. Notably, the characteristic absorption peak shifts to a lower wavenumber as the size of nano-$SiO_2$ increases, indicating that larger nanoparticles form stronger interfacial bonds with the hydrogel matrix. Meanwhile, we performed peak deconvolution on the absorption band around 3300 $cm^{-1}$ in the FTIR spectra of composite hydrogels with the same particle size but varying silica contents (Fig. S15 in ESI). The band was deconvoluted into 2 bands at 3370 and 3210 $cm^{-1}$, which are attributed to the stretching vibration of free hydroxyl groups and the stretching vibration of hydrogen-bonded hydroxyl groups between PVA chains, respectively. Based on the relative area ratios of these peaks, as the silica content increases, the intensity of the absorption band at 3370 $cm^{-1}$ gradually decreases, while the proportion of the absorption band at 3210 $cm^{-1}$ progressively increases, indicating that the incorporation of $SiO_2$ enhances hydrogen bonding interaction. This observation also accounts for the significant enhancement in mechanical and swelling properties imparted by larger nanoparticles, as demonstrated in Figs. 2 and 3. Although larger nano-silica particles exhibit a relatively small specific surface area, smaller nanoparticles tend to undergo localized agglomeration under critical filling conditions when approaching maximum loading, thereby restricting their effective interaction with PVA hydrogels. In contrast, the composite strategy presented in this study facilitates more effective dispersion of larger nano-$SiO_2$ particles. The surface hydroxyl groups of the nano-$SiO_2$ form a dense hydrogen-bonding network with the abundant hydroxyl groups present in the PVA hydrogel, thereby achieving strong interfacial bonding within the composite material. Meanwhile, the DSC curves of the PVA/$SiO_2$ composite hydrogel (Fig. 5j) reveal a gradual increase in the glass transition temperature ($T_g$) with increasing nanofiller content. This trend suggests that higher nanoparticle loading promotes strong physical interactions with the PVA chains, thereby restricting their mobility. This result confirms the formation of robust interfacial bonding between the PVA matrix and the nano-$SiO_2$ particles.

Finally, the water content of the samples was estimated by comparing the thermogravimetric analysis (TGA) curves before and after swelling (Fig. 5k and Fig. S16 in ESI), based on the weight loss attributable to water evaporation below 200 °C. Prior to swelling, the high-density PVA/$SiO_2$ composite hydrogel (500 nm, 6 wt%) exhibited a water content of approximately 40.71 wt%. As the nano-silica content increased, the water content of the composite hydrogels gradually decreased. After reaching swelling equilibrium in deionized water, the high-density PVA/$SiO_2$ composite hydrogel (500 nm, 6 wt%) exhibits a significant increase in water content, reaching 65.47 wt%. This water content is consistent with observations from SEM morphology, indicating that by altering the swelling environment, both the water content and the microstructure of the composite hydrogel can be effectively modulated across a broad range.

In summary, the high-density PVA/$SiO_2$ composite hydrogel effectively optimizes the stress field distribution by reducing the modulus mismatch between the hydrogel matrix and the reinforcing phase *via* increasing polymer chain density. Coupled with strong hydrogen bonding at the PVA-$SiO_2$ interface, this design promotes uniform stress transfer, resulting in a material that exhibits both high strength and high toughness. It significantly enhances energy dissipation efficiency through a $SiO_2$ phase-induced nonlinear crack propagation mechanism, while simultaneously achieving exceptional notch resistance. Leveraging a dynamic and reversible interface regulation mechanism, this system exhibits controllable swelling behavior and facilitates broad modulation of its mechanical properties through a solvent exchange strategy. This versatility allows it to meet a wide spectrum of practical demands. The high-density PVA/$SiO_2$ composite hydrogel is highly advantageous for fabricating mechanical protective materials due to its outstanding comprehensive properties. Additionally, its distinctive mechanical properties combined with excellent tunability position it as a key enabler in cutting-edge fields including flexible sensors and intelligent actuators, thereby advancing the development of high-performance functional materials through new insights and technical pathways.

## CONCLUSIONS

Based on the innovative design concept of "blending fillers in the viscoelastoplastic state and fixing the structure in the viscoelastic state," this study establishes a versatile and efficient strategy for fabricating high-performance composite hydrogels. The proposed methodology provides three key advantages over conventional approaches. First, mechanical mixing in the viscoelastoplastic state effectively mitigates filler aggregation, significantly expanding the range of viable blending phases. Second, the high polymer chain density and abundant physical interactions inherent to the viscoelastoplastic matrix markedly reduce modulus mismatch with dispersed phases, thereby addressing the persistent challenge of weak interfacial adhesion. Third, superior interfacial strength is achieved through a synergistic combination of intrinsic rich interactions of viscoelastoplastic hydrogel, physical filler-matrix bonding, and secondary reorganization of interactions during viscoelastic molding. These structural advantages facilitate robust interfacial bonding, which promotes crack front deflection and tortuous crack propagation under load, enabling efficient energy dissipation and significantly enhancing crack-propagation resistance. As a result, the developed PVA/$SiO_2$ composite hydrogels exhibit outstanding mechanical properties and long-term stability, demonstrating great potential for demanding mechanical protection applications. This work provides both a fundamental principle and a practical pathway for designing and fabricating advanced hydrogel composites with superior mechanical properties.

### Conflict of Interests

The authors declare no interest conflict.

### Electronic Supplementary Information

Electronic supplementary information (ESI) is available free of charge in the online version of this article at http://doi.org/10.1007/s10118-025-3547-8.

## Data Availability Statement

The data that support the findings of this study are available from the corresponding authors upon reasonable request.

## ACKNOWLEDGMENTS

This work was financially supported by the Natural Science Foundation of Shandong Province (No. ZR2023YQ042) and the National Natural Science Foundation of China (No. 22273042).

## REFERENCES

1 Zhao, C. X.; Guo, M.; Mao, J.; Li, Y. T.; Wu, Y. P.; Guo, H.; Xiang, D.; Li, H. Self-healing, stretchable, temperature-sensitive and strain-sensitive hydrogel-based flexible sensors. *Chinese J. Polym. Sci.* **2023**, *41*, 334–344.
2 Zhao, L. J.; Tang, N.; Wang, X. T.; Li, M. H.; Hu, J. Conductive polyaniline hydrogel featuring high toughness and low hysteresis. *Chinese J. Polym. Sci.* **2025**, *43*, 581–587.
3 Feng, Y. B.; Liu, H.; Zhu, W. H.; Guan, L.; Yang, X. T.; Zvyagin, A.; Zhao, Y.; Shen, C.; Yang, B.; Lin, Q. Muscle-inspired MXene conductive hydrogels with anisotropy and low-temperature tolerance for wearable flexible sensors and arrays. *Adv. Funct. Mater.* **2021**, *31*, 2105264.
4 Li, X. T.; Zhang, S. Q.; Li, X. A.; Lu, L.; Cui, B.; Yuan, C.; Guo, L.; Yu, B.; Chai, Q. Q. Starch/polyvinyl alcohol with ionic liquid/graphene oxide enabled highly tough, conductive and freezing-resistance hydrogels for multimodal wearable sensors. *Carbohydr. Polym.* **2023**, *320*, 121262.
5 Li, Y.; Zhu, C. H.; Fan, D. D.; Fu, R. Z.; Ma, P.; Duan, Z. G.; Li, X.; Lei, H.; Chi, L. A bi-layer PVA/CMC/PEG hydrogel with gradually changing pore sizes for wound dressing. *Macromol. Biosci.* **2019**, *19*, 1800424.
6 Wang, C.; Liu, Y.; Qu, X. C.; Shi, B. J.; Zheng, Q.; Lin, X. B.; Chao, S. Y.; Wang, C. Y.; Zhou, J.; Sun, Y.; Mao, G. S.; Li, Z. Ultra-stretchable and fast self-healing ionic hydrogel in cryogenic environments for artificial nerve fiber. *Adv. Mater.* **2023**, *35*, 2300757.
7 Pan, S.; Xia, M.; Li, H.; Jiang, X.; He, P.; Sun, Z.; Zhang, Y. Transparent, high-strength, stretchable, sensitive and anti-freezing poly(vinyl alcohol) ionic hydrogel strain sensors for human motion monitoring. *J. Mater. Chem. C.* **2020**, *8*, 2827–2837.
8 Li, R.; Shi, Y.; Alsaedi, M.; Wu, M.; Shi, L.; Wang, P. Hybrid hydrogel with high water vapor harvesting capacity for deployable solar-driven atmospheric water generator. *Environ. Sci. Technol.* **2018**, *52*, 11367–11377.
9 Guo, Z.;Wang, Z.;Pan, W.;Zhang, J.;Qi, Y.;Qin, Y.;Zhang, Y. Fiber-reinforced polyvinyl alcohol hydrogel *via in situ* fiber formation. *E-Polymer* **2023**, *23*, 20230056.
10 Wang, M.; Bai, J.; Shao, K.; Tang, W.; Zhao, X.; Lin, D.; Huang, S.; Chen, C.; Ding, Z.; Ye, J. Poly(vinyl alcohol) hydrogels: the old and new functional materials. *Int. J. Polym. Sci.* **2021**, *2021*, 2225426.
11 Liu, Y. G.; Zhang, J.; Wang, D. Y. Preparation schemes and

## Graphical Abstract

**Strong and Tough Composite Hydrogels with Crack-deflecting Ability Enabled by a Viscoelastoplastic Mixing Strategy**

Xiang Li, Bei Jiang, Bin Wang, Ya-Rong Yang, Gui-Ming Zhao, and Li-Li Wang

*Qingdao University*

A novel strategy of "blending reinforcement in the viscoelastoplastic state and structural fixation in the viscoelastic state" was developed to fabricate poly(vinyl alcohol) (PVA)/silica composite hydrogels. This approach results in enhanced interfacial strength and a high-density polymer network, thereby endowing the hydrogels with outstanding mechanical properties and long-term stability.

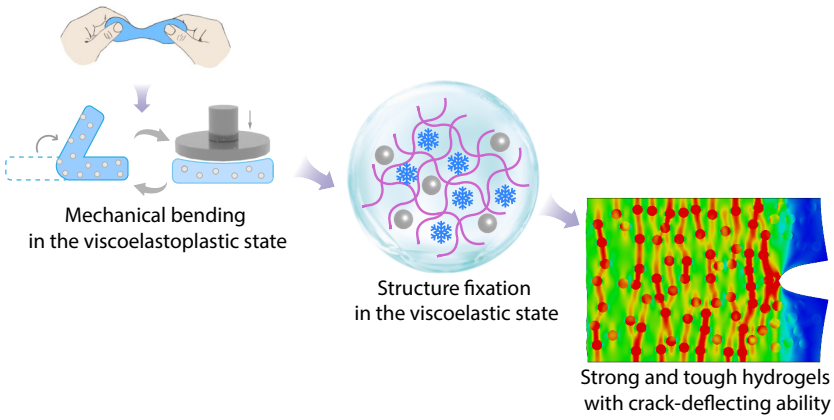


*Chinese J. Polym. Sci. 2026, 44, 768–780* *https://doi.org/10.1007/s10118-025-3547-8*

applications of multifunctional PVA composite hydrogels. *Chem. Eng. J.* **2025**, *508*, 160946.
12 Zhao, G. M.; Li, X.; Zhang, X. S.; Chen, L. C.; Yuan, L. H.; Dong, X.; Wang, L. L.; Surfactant-driven bidirectional tuning of viscoplastic physical hydrogels and the underlying mechanism. *Macromolecules* **2025**, *58*, 12117–12127.
13 Seo, Y.; Lee, J.; Park, S.; Kim, M.; Kim, S.; Oh, T. PVA hydrogels supplemented with PLA mesh for tissue regeneration scaffold. *Gels.* **2024**, *10*, 364.
14 Xu, R. D.; She, M. H.; Liu, J. X.; Zhao, S. K.; Zhao, J. S.; Zhang, X. J.; Qu, L. J.; Tian, M. W. Skin-friendly and wearable iontronic touch panel for virtual-real handwriting interaction. *ACS Nano.* **2023**, *17*, 8293–8302.
15 Feng, X.; Tian, Y.; Gu, G.; Wang, C.; Shang, S.; Huang, X.; Jiang, J.; Song, Z.; Zhang, H. High-strength PVA/cellulosic hydrogels with acid/base and thermo dual-responsive fluorescence. *Chem. Eng. J.* **2024**, *500*, 156763.
16 Li, Z.; Jiang, J.; Luo, J.; Meng, J.; Cheng, L.; Qin, H. A robust and conductive hydrotalcite/nanocellulose/PVA hydrogel constructed based on the Hofmeister effect. *Int. J. Biol. Macromol.* **2025**, *298*, 139994.
17 Piacentini, E.; Poerio, T.; Bazzarelli, F.; Giorno, L. Continuous production of PVA-based hydrogel nanoparticles by membrane nanoprecipitation. *J. Membr. Sci.* **2021**, *637*, 119649.
18 Hu, M.; Gu, X. Y.; Hu, Y.; Deng, Y. H.; Wang, C. Y. PVA/carbon dot nanocomposite hydrogels for simple introduction of Ag nanoparticles with enhanced antibacterial activity. *Macromol. Mater. Eng.* **2016**, *301*, 1352–1362.
19 Lorusso, E.; Ali, W.; Hildebrandt, M.; Mayer-Gall, T.; Gutmann, J. Hydrogel functionalized polyester fabrics by UV-induced photopolymerization. *Polymers.* **2019**, *11*, 1329.
20 Qin, Z. P.; Zhao, G.; Zhang, Y. Y.; Gu, Z. H.; Tang, Y. H.; Aladejana, J. T.; Ren, J. N.; Jiang, Y. H.; Guo, Z. H.; Peng, X. F.; Zhang, X. H.; Xu, B. B.; Chen, T. J. A simple and effective physical ball-milling strategy to prepare super-tough and stretchable PVA@MXene@PPy hydrogel for flexible capacitive electronics. *Small.* **2023**, *19*, 2303038.
21 Wu, M.; Peng, Q. Y.; Han, L. B.; Zeng, H. B. Self-healing hydrogels and underlying reversible intermolecular interactions. *Chinese J. Polym. Sci.* **2021**, *39*, 1246–1261.
22 Zhou, Y.; Wan, C. J.; Yang, Y. S.; Yang, H.; Wang, S. C.; Dai, Z. D.; Ji, K. J.; Jiang, H.; Chen, X. D.; Long, Y. Highly stretchable, elastic, and ionic conductive hydrogel for artificial soft electronics. *Adv. Funct. Mater.* **2019**, *29*, 1806220.
23 Jiang, B.; Nie, Z. P.; Zhao, G. M.; Wang, B.; Xu, H. X.; Zhang, X. S.; Wang, L. L. Matching combination of amorphous ionic hydrogel with elastic fabric enables integrated properties for wearable sensing. *Polymer.* **2024**, *315*, 127790.
24 Xu, R. D.; Qu, L. J.; Tian, M. W. Touch-sensing fabric encapsulated with hydrogel for human-computer interaction. *Soft Matter.* **2021**, *17*, 9014–9018.
25 Guan, Q. F.; Yang, H. B.; Han, Z. M.; Ling, Z. C.; Yin, C. H.; Yang, K. P.; Zhao, Y. X.; Yu, S. H. Sustainable cellulose-nanofiber-based hydrogels. *ACS Nano* **2021**, *15*, 7889–7898.
26 Hubbard, A. M.; Cui, W.; Huang, Y. W.; Takahashi, R.; Dickey, M. D.; Genzer, J.; King, D. R.; Gong, J. P. Hydrogel/elastomer laminates bonded *via* fabric interphases for stimuli-responsive actuators. *Matter.* **2019**, *1*, 674–689.
27 Zhang, N.; Zhang, B.; Pang, Y.; Yang, H. S.; Zong, L.; Duan, Y. X.; Zhang, J. M. High performance of PVA nanocomposite reinforced by Janus-like asymmetrically oxidized graphene: synergetic effect of H-bonding interaction and interfacial crystallization. *Chinese J. Polym. Sci.* **2022**, *40*, 373–383.
28 Ren, J.; Yang, X.; Xiang, X. Carboxymethyl cellulose-reinforced sandwich-structured carbon nanotube composite hydrogels for strain sensing and joule heating. *Carbohydr. Polym.* **2025**, *369*, 124291.
29 Ratwani, C.; Zhao, S.; Huang, Y.; Hadfield, M.; Kamali, A.; Abdelkader, A. Surface modification of transition metal dichalcogenide nanosheets for intrinsically self-healing hydrogels with enhanced mechanical properties. *Small.* **2023**, *19*, 2207081.
30 Zhang, R.; Wu, Y.; Lin, P.; Jia, Z. F.; Zhang, Y. J.; Liu, F. Z.; Yu, B.; Zhou, F. Extremely tough hydrogels with cotton fibers reinforced. *Adv. Eng. Mater.* **2020**, *22*, 2000508.
31 Sun, M. Z.; Li, H. G.; Hou, Y.; Huang, N.; Xia, X. Y.; Zhu, H. J.; Xu, Q.; Lin, Y.; Xu, L. Z. Multifunctional tendon-mimetic hydrogels. *Sci. Adv.* **2023**, *9*, eade6973.
32 Arno, M. C.; Inam, M.; Weems, A. C.; Li, Z. H.; Binch, A. L. A.; Platt, C. I.; Richardson, S. M.; Hoyland, J. A.; Dove, A. P.; O'Reilly, R. K. Exploiting the role of nanoparticle shape in enhancing hydrogel adhesive and mechanical properties. *Nat. Commun.* **2020**, *11*, 1420.
33 Zhang, X. Y.; Deng, S, Y.; Cai, C, M.; Li, J, C.; Lei, C. H.; Chen, A. F.; Gao, Y. F. Preparation and viscoelastic behavior of hydrogel composites. *Acta Polymerica Sinica* (in Chinese) **2025**, 56, 1215–1222.